Physics of Fluids

Hydrostatic pressure and interfacial tension induce mode instability in wave propagation along a liquid-filled microtubule

Yufei Wu (吴宇飞), Moxiao Li (李墨筱), Jun Yin (殷俊), Shaobao Liu (刘少宝) (iD), and Tian Jian Lu (卢天健)

COLLECTIONS

Paper published as part of the special topic on Advances in Micro/Nano Fluid Flows: In Memory of Prof. Jason Reese and Collection

View Online   Export Citation   CrossMark

Hydrostatic pressure and interfacial tension induce mode instability in wave propagation along a liquid-filled microtubule

Yufei Wu (吴宇飞),[1,2] **Moxiao Li (李墨筱),**[1,2] **Jun Yin (殷俊),**[2,3] **Shaobao Liu (刘少宝),**[2,3,a] [ID] **and Tian Jian Lu (卢天健)**[2,3,a]

AFFILIATIONS

[1] State Key Laboratory for Strength and Vibration of Mechanical Structures, School of Aerospace,
Xi'an Jiaotong University, Xi'an 710049, People's Republic of China
[2] State Key Laboratory of Mechanics and Control of Mechanical Structures, Nanjing University of Aeronautics and Astronautics,
Nanjing 210016, People's Republic of China
[3] Nanjing Center for Multifunctional Lightweight Materials and Structures, Nanjing University of Aeronautics and Astronautics,
Nanjing 21006, China

[a] Authors to whom correspondence should be addressed: sbliu@nuaa.edu.cn and tjlu@nuaa.edu.cn

ABSTRACT

Wave propagation in microtubules plays an important role in cell function and engineering applications. Interfacial tension and hydrostatic pressure significantly affect such wave propagation in liquid-filled microtubules, but it remains elusive how they influence the dispersion relation. To address this, we develop a theoretical model based on Flügge's theory, with interfacial tension and hydrostatic pressure duly accounted for. We then employ the model to analyze the dispersion relation of axisymmetric and non-axisymmetric waves. The difference between interfacial tension and hydrostatic pressure is found to affect the dispersion relation. With the increase in interfacial tension, wave velocity increases for all modes of axisymmetric waves under different hydrostatic pressures. With the increase in interfacial tension or decrease in hydrostatic pressure, wave velocity increases for the first mode of the non-axisymmetric wave but non-monotonously changes for the second and third modes of the non-axisymmetric wave. Notably, increasing the difference between dimensionless hydrostatic pressure (μ) and dimensionless interfacial tension (λ) can lead to mode instability. For the axisymmetric wave, the second mode becomes unstable when $|\mu-\lambda|$ is sufficiently large. For the non-axisymmetric wave, the first mode becomes unstable when $|\mu-\lambda|$ is large enough and the second mode becomes unstable only when $\mu-\lambda$ is positive and large enough. The developed theory enables a better understanding of the effect of the environment on signal transmission in cells and provides guidelines in nondestructive testing with microtubules.

I. INTRODUCTION

Microtubules are filamentous structures composed of a hollow cylinder of tubulin subunits (α, β, and their isoforms),[1,2] which are basic structural and functional units involved in cell signaling, cell shape maintenance, cell transport, cell motility, and cell division.[3–5] Wave propagation in microtubules is important in both cell function and bioengineering applications. In cell signaling, microtubules are important parts of axons, which play a key role in the propagation of action potential accompanied by mechanical waves.[6,7] In cell division, microtubules mediate the waves of cytoplasm reorganization, which reflects the appearance and spreading of mitotic activity.[8] Radial microtubule systems are important in the propagation of successive mitotic waves, which are significant in plant morphogenesis.[9] In cell mobility, the wave propagates along microtubules in the movement of cells by flagella and cilia, where microtubules function as transmission lines.[10,11] Furthermore, understanding wave propagation in microtubules is helpful in its application as an ultrasonic contrast agent in ultrasound imaging.[12] It is also helpful in non-destructive detection to determine the viscoelastic properties of structures in cells.[13,14]

Continuum mechanics is a common and applicable method to describe the mechanical behavior of microtubules (longer than 0.5 μm).[15,16] The validity of continuum mechanics can be

examined by several numerical methods such as the lattice model[17] and the molecular structural mechanics method.[18] The elastic parameters measured in experiments are able to describe the bending, shear, and compression of microtubules.[16] Based on the continuum mechanics approach, several theoretical models were developed to characterize the properties of wave propagation in cellular microtubules. Isotropic elastic beam models have been used to study the buckling behavior of microtubules in terms of flexural rigidity.[19,20] However, elastic beam models cannot describe the shell-like two-dimensional (2D) behavior of hollow microtubules, e.g., shell-like buckling[15,21] and vibration modes.[22] In addition, microtubules exhibit strong anisotropy.[23,24] Based on Flügge's shell theory and the orthotropic constitutive relation, both axisymmetric and non-axisymmetric waves in free microtubules have been studied[17,25] and the validity of the shell model for dispersion relation of microtubules is verified by comparison with known results obtained from the lattice model.[17] Wave propagation in microtubules embedded in elastic medium has also been studied, as stiffening of the elastic medium increases the flexural rigidity of microtubules.[26] In a real situation, however, microtubules are always in a liquid environment with hydrostatic pressure, e.g., $p = 770$ kPa.[27] Besides, surface tension, e.g., $\sigma = 0.072$ N/m,[28] needs to be considered for microtubules typically with outer diameter $d_o \approx 24$ nm and inner diameter $d_i \approx 12$ nm.[29] These two factors are expected to have an important influence on the dispersion relation of wave propagation.[30–33] However, there is yet a study on the effects of interfacial tension and hydrostatic pressure on the dispersion properties of wave propagation in microtubules.

In the current study, based on Flügge's shell theory, the governing equation of a microtubule is developed by introducing relevant terms concerning hydrostatic pressure and interfacial tension. Frequency dispersions (i.e., relation between wave velocity and wave number) of both axisymmetric and non-axisymmetric waves in microtubules are determined by systematically varying the interfacial tension and hydrostatic pressure. The proposed theory enables

better understanding and prediction of the dispersion properties of wave propagation in liquid-filled microtubules.

II. THEORETICAL ANALYSIS

A. Governing equations

Microtubules are filamentous structures involved in many aspects of cell structure, motility, and transport. A microtubule is composed of a hollow cylinder of tubulin subunits (α, β, and their isoforms), which are arranged in a polar fashion along 13 protofilaments in the axial direction[1,2] [Fig. 1(a)]. As a result, the microtubule exhibits strong anisotropic properties.[3–5] The microtubule is filled with uniquely arranged water molecules.[34,35] As these molecules are confined, the fluid is hard to flow, thus causing no flutter and instability in the microtubule. At the size of a microtubule (outer diameter $d_o \approx 24$ nm and inner diameter $d_i \approx 12$ nm), water inside is bulk-like liquid phase.[36,37] In addition, for nanoscale capillaries, the liquid–solid interfacial tension (σ) is not negligible. In some cases (e.g., metaphase and anaphase of mitosis), two ends of the microtubule are attached to chromosome and centrosome, respectively, which forms a closed tube,[38,39] to achieve their function. Due to the change of environment of the cytoplasm, the outer pressure will differ from the pressure inside the microtubule. Therefore, there will be hydrostatic pressure (p) caused by the difference between inner and outer pressure. In the current study, based on Flügge's shell theory,[17,25,40] a modified orthotropic shell model is developed to describe a liquid-filled microtubule, with interfacial tension and hydrostatic pressure accounted for.

We set the interfacial tension coefficient to be σ and the mean radius of the microtubule to be R. The inner and outer interfacial tension plays the role of a uniform radial tensile force $\frac{2\sigma}{R}$ around the microtubule cross section (yielding a hoop force 2σ) and initial stress in the x direction [Figs. 1(b) and 1(c)]. At nanoscale, we assume that the liquid is attached to the wall of the microtubule
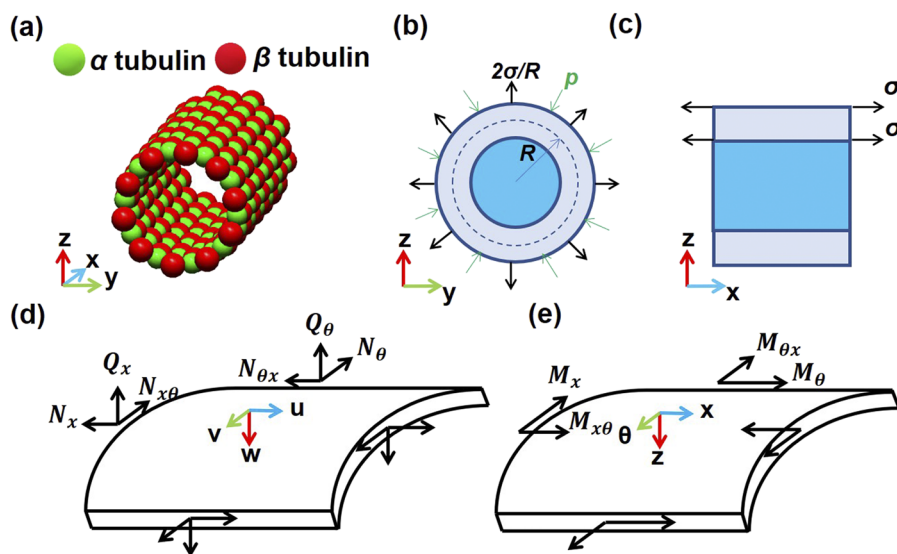

FIG. 1. (a) Sketch of a microtubule-like capillary tube. [(b) and (c)] Sketch of interfacial tension and hydrostatic pressure in a liquid-filled microtubule. σ is the interfacial tension between microtubule and the liquid in it. According to the Young–Laplace equation,[71] the radial force due to the inner and outer interfacial tension is $\frac{2\sigma}{R}$. (d) Sketch of internal forces in a micro-element, with u, v, and w denoting the direction of displacement. (e) Sketch of internal moments in a micro-element, with N_x, N_θ, $N_{x\theta}$, $N_{\theta x}$, Q_θ, Q_x, M_x, M_θ, $M_{x\theta}$, $M_{\theta x}$ describing forces and moments per unit length acting on the sides of a shell element.

and is unable to move freely, and thus no inner pressure is induced. Considering the hydrostatic pressure p, which generates a hoop force in the shell, we write the initial internal forces in the shell as

$$N_{\theta I} = -pR + 2\sigma, \tag{1a}$$

$$N_{xI} = 2\sigma, \tag{1b}$$

where p is the hydrostatic pressure, and $N_{\theta I}$ and N_{xI} represent the initial internal forces in θ and x directions, respectively. Using $\bar{N}$ with superscript to represent the total forces, we can get

$$\overline{N_\theta} = N_{\theta I} + N_\theta = -pR + 2\sigma + N_\theta, \tag{2a}$$

$$\overline{N_x} = N_{xI} + N_x = 2\sigma + N_x, \tag{2b}$$

$$\overline{N_{x\theta}} = N_{x\theta I} + N_{x\theta} = N_{x\theta}, \tag{2c}$$

$$\overline{N_{\theta x}} = N_{\theta x I} + N_{\theta x} = N_{\theta x}. \tag{2d}$$

Here, $N_\theta, N_x, N_{x\theta}$, and $N_{\theta x}$ are the additional forces caused by wave propagation and have elastic relations with the additional displacements u, v, and w caused by wave propagation compared with the situation without wave propagation [Figs. 1(d) and 1(e)]. The x-y-z coordinate is a global coordinate introduced to describe the whole microtubule so that Figs. 1(a)–1(c) look clearer. In the following theoretical analysis, however, the x-θ-z coordinate is adopted as a local coordinate to characterize an arbitrary micro-element of the microtubule [Figs. 1(d) and 1(e)].

By Newton's second law and the constitutive law of orthotropic shells,[41,42] the governing equation for a liquid-filled microtubule can be given as

$$\left\{ \left(\frac{2\sigma R^2}{K_x} + R^2 \right) \frac{\partial^2}{\partial x^2} + \left(\frac{K_{x\theta} R^2 + D_{x\theta} + 2\sigma R^2 - pR^3}{R^2 K_x} \right) \frac{\partial^2}{\partial \theta^2} \right\} u + \left\{ \frac{R(v_x K_\theta + K_{x\theta})}{K_x} \frac{\partial^2}{\partial x \partial \theta} \right\} v$$

$$+ \left\{ \left(\frac{2\sigma R - R v_x K_\theta - pR^2}{K_x} \right) \frac{\partial}{\partial x} + \frac{RD_x}{K_x} \frac{\partial^3}{\partial x^3} - \frac{D_{x\theta}}{RK_x} \frac{\partial^3}{\partial x \partial \theta^2} \right\} w = \frac{\rho h}{K_x} R^2 \frac{\partial^2 u}{\partial t^2}, \tag{3a}$$

$$\left\{ R \left(v_\theta + \frac{K_{x\theta}}{K_x} \right) \frac{\partial^2}{\partial x \partial \theta} \right\} u + \left\{ \frac{K_\theta + 2\sigma - pR}{K_x} \frac{\partial^2}{\partial \theta^2} + \frac{(K_{x\theta} R^2 + 3D_{x\theta} + 2\sigma R^2)}{K_x} \frac{\partial^2}{\partial x^2} \right\} v$$

$$+ \left\{ \frac{pR - 2\sigma - K_\theta}{K_x} \frac{\partial}{\partial \theta} + \left(\frac{v_\theta D_x + 3D_{x\theta}}{K_x} \right) \frac{\partial^3}{\partial x^2 \partial \theta} \right\} w = \frac{\rho h}{K_x} R^2 \frac{\partial^2 v}{\partial t^2}, \tag{3b}$$

$$\left\{ \frac{(K_x v_\theta R + pR^2 - 2\sigma R)}{K_x} \frac{\partial}{\partial x} - R \frac{D_x}{K_x} \frac{\partial^3}{\partial x^3} + \frac{D_{x\theta}}{RK_x} \frac{\partial^3}{\partial x \partial \theta^2} \right\} u + \left\{ \left(\frac{K_\theta - pR + 2\sigma}{K_x} \right) \frac{\partial}{\partial \theta} - \frac{(v_x D_\theta + 3D_{x\theta})}{K_x} \frac{\partial^3}{\partial x^2 \partial \theta} \right\} v$$

$$+ \left\{ -R^2 \frac{D_x}{K_x} \frac{\partial^4}{\partial x^4} - \left(\frac{v_x D_\theta + v_\theta D_x + 4D_{x\theta}}{K_x} \right) \frac{\partial^4}{\partial x^2 \partial \theta^2} + \frac{2\sigma R^2}{K_x} \frac{\partial^2}{\partial x^2} - \frac{D_\theta}{R^2 K_x} \frac{\partial^4}{\partial \theta^4} - \frac{2D_\theta + 2\sigma R^2 - pR^3}{R^2 K_x} \frac{\partial^2}{\partial \theta^2} - \left(\frac{D_\theta}{R^2 K_x} + \frac{K_\theta}{K_x} \right) \right\} w$$

$$= \frac{\rho h}{K_x} R^2 \frac{\partial^2 w}{\partial t^2}. \tag{3c}$$

Here, x and θ are the axial coordinate and circumferential angular coordinate, respectively, u, v, and w are the additional axial displacement, circumferential displacement, and radial (inward positive) deflection caused by wave propagation, ρ is the mass density, and R is the average radius of the microtubule. Furthermore, K_x, $K_{x\theta}$, and K_θ are the extensional rigidity, and D_x, D_θ, and $D_{x\theta}$ are the flexural rigidity, which satisfy $K_x = \frac{E_x h}{1 - v_x v_\theta}$, $K_\theta = \frac{E_\theta h}{1 - v_x v_\theta}$, $K_{x\theta} = G_{x\theta} h$, $D_x = \frac{E_x h_0^3}{12(1 - v_x v_\theta)}$, $D_\theta = \frac{E_\theta h_0^3}{12(1 - v_x v_\theta)}$, and $D_{x\theta} = \frac{G_{x\theta} h_0^3}{12}$. h is the equivalent thickness for tension and compression; h_0 is another effective thickness for bending. E_x is the longitudinal modulus, E_θ is the circumferential modulus, $G_{x\theta}$ is the shear modulus, and v_x is the Poisson ratio along the longitudinal direction. The Poisson ratio v_θ along the circumferential direction can be determined by $v_\theta / v_x = E_\theta / E_x$.

B. Dispersion equations

We assume the wave in a microtubule to be a traveling wave. Mathematically, it is described by $u_i = U_i g_i(n\theta) f_i(k_x x - \omega t)$, where $i = 1, 2, 3$ represents the direction x, y, and z, U_i is the amplitude of the wave component in the i direction, and n is the circumferential wave number representing the degree of non-asymmetry. According to the value of n, two forms of wave can be obtained: when $n = 0$, an axisymmetric wave is obtained, which means that the wave form is not related to θ; when $n > 0$, a non-axisymmetric wave is obtained in which the wave form depends on θ.

1. Axisymmetric wave

The axisymmetric solution to Eq. (3) is independent of θ, which can be written as

$$u(x,t) = U \sin(k_x x - \omega t), \quad (4a)$$

$$v(x,t) = V \cos(k_x x - \omega t), \quad (4b)$$

$$w(x,t) = W \cos(k_x x - \omega t), \quad (4c)$$

where the displacements in all three directions are independent of coordinate θ. Substituting them into Eq. (3), we can get

$$\left[(1+\lambda)k^2 - \Omega^2\right]U + k(\lambda - \mu - \alpha v_x - \gamma k^2)W = 0, \quad (5a)$$

$$\left\{\Omega^2 - k^2[\beta(1+3\gamma) + \lambda]\right\}V = 0, \quad (5b)$$

$$\left[(\alpha v_x + \mu - \lambda)k + \gamma k^3\right]U + \left[\Omega^2 - \gamma k^4 - \lambda k^2 - \alpha(\gamma+1)\right]W = 0, \quad (5c)$$

in which $\alpha = \frac{v_\theta}{v_x} = \frac{E_\theta}{E_x} = \frac{K_\theta}{K_x} = \frac{D_x}{D_\theta}$, $\beta = \frac{G_{x\theta}}{E_x} \approx \frac{G_{x\theta}}{E_x(1-\alpha v_x^2)} = \frac{D_{x\theta}}{D_x} = \frac{K_{x\theta}}{K_x}(\alpha v_x^2 \to 0)$ are separately the ratio of circumferential to longitudinal moduli and the ratio of shear to longitudinal moduli, which characterize the anisotropy of the microtubule, $\gamma = \frac{h_0^3}{12hr^2}$, and $S_L = \sqrt{\frac{K_x}{\rho h}} \approx \sqrt{\frac{E_x}{\rho}}$ is the longitudinal sound speed. $\lambda = \frac{2\sigma}{K_x}$, $\mu = \frac{pR}{K_x}$, $\Omega = \frac{\omega}{S_L}$, and $k = Rk_x$ are the dimensionless interfacial tension, dimensionless hydrostatic pressure, dimensionless frequency, and dimensionless wave number, respectively.

Equation (5b) is decoupled from the other two, leading to the velocity of torsional waves,

$$c_t = S_L\sqrt{\beta(1+3\gamma) + \lambda}. \quad (6)$$

This is similar to that of shearing waves in an infinite medium, $c_T = \sqrt{\frac{G_{x\theta}}{\rho}}$.

The other two equations of (5) can be expressed as

$$A(k,\Omega)_{2\times 2}(U,W)^T = 0. \quad (7)$$

For non-trivial solution of the equation, we arrive at

$$\mathrm{Det}\left[A(k,\Omega)_{2\times 2}\right] = 0. \quad (8)$$

Equations (6) and (8) are the dispersion equations.

2. Non-axisymmetric waves

The non-axisymmetric solution to Eq. (3) can be written as

$$u(x,t) = U \sin(k_x x - \omega t)\cos n\theta, \quad (9a)$$

$$v(x,t) = V \cos(k_x x - \omega t)\sin n\theta, \quad (9b)$$

$$w(x,t) = W \cos(k_x x - \omega t)\cos n\theta. \quad (9c)$$

Substitution of (9) into (3) yields

$$\left\{(1+\lambda)k^2 - \Omega^2 + [\beta(1+\gamma) + \lambda - \mu]n^2\right\}U$$
$$+ k(\alpha v_x + \beta)nV + k(\lambda - \mu - \alpha v_x - \gamma k^2 + \beta\gamma n^2)W = 0, \quad (10a)$$

$$[-k(\alpha v_x + \beta)n]U + \left\{\Omega^2 - k^2[\beta(1+3\gamma) + \lambda] - (\alpha + \lambda - \mu)n^2\right\}V$$
$$+ [k^2\gamma(\alpha v_x + 3\beta)n - (\mu - \lambda - \alpha)n]W = 0, \quad (10b)$$

$$\left[(\alpha v_x + \mu - \lambda)k + \gamma k^3 - \beta\gamma kn^2\right]U + \left[(\alpha + \lambda - \mu)n + \gamma k^2(\alpha v_x + 3\beta)n\right]V$$
$$+ \left[\Omega^2 - \gamma k^4 - \lambda k^2 - 2\gamma(\alpha v_x + 2\beta)k^2 n^2 - \alpha\gamma n^4\right.$$
$$\left. + (2\alpha\gamma + \lambda - \mu)n^2 - \alpha(\gamma+1)\right]W = 0. \quad (10c)$$

These equations can be written as

$$B(n,k,\Omega)_{3\times 3}(U,V,W)^T = 0, \quad (11)$$

from which the dispersion equation is given by

$$\mathrm{Det}\left[B(n,k,\Omega)_{3\times 3}\right] = 0. \quad (12)$$

The dispersion equations [(8) and (12)] can be solved numerically by MATLAB. The ranges of material constants for microtubules are listed in Table I. In our numerical solution, we set the parameters as $R = 12.8$ nm, $E_x = 1$ GPa, $E_\theta = 1$ MPa, $G_{x\theta} = 1$ MPa, $v_x = 0.3$, $\rho = 1.47$ g/cm^3, $h = 2.7$ nm, $h_0 = 1.6$ nm, $\alpha = 0.001$, $\beta = 0.001$, and $\gamma = 0.0008$.

III. RESULTS

A. Axisymmetric wave

Phase velocity is the rate at which the phase of the wave propagates in space (i.e., the velocity of one harmonic wave in the wave packet). In this study, we focus on individual modes of the waves in which phase velocity is an appropriate property. Besides, to explore the dispersion relation, the phase velocity is commonly studied in the existing literature of wave propagation.[25,26,43] Admittedly, there are other properties such as the group velocity that usually used to describe the velocity of energy propagation. These other properties related to wave propagation will be studied in our future work.

Solving Eqs. (6) and (8), we can get the dispersion relation about phase velocity of three different modes for varying values of interfacial tension and hydrostatic pressure. Since we care about the stable modes that will not attenuate or diverge along the propagating path, we only deal with the solution with real dimensionless

---

wave number k. In this situation, the phase wave velocity can be expressed as $c = \frac{\omega}{k_x}$. Thus, we can get the wave velocity c as a function of k.

Equation (5b) is decoupled from Eqs. (5a) and (5c), which gives the velocity of the first mode wave [Eq. (6)]. The velocity of the first mode is dependent upon interfacial tension but independent of hydrostatic pressure. Besides, the velocity does not change with k, which shows no frequency dispersion. With the increase in interfacial tension, the velocity of the torsional mode will increase [Figs. 2(a)–2(d)]. In fact, these results can also be obtained from Eq. (6).

For the other two modes, the dependence of mode velocity upon dimensionless wave number k can be solved from Eq. (8) analytically, as detailed in the supplementary material. In the absence of interfacial tension and hydrostatic pressure (i.e., $\mu = 0$ and

$\lambda = 0$), the wave velocity coincides well with that reported in the literature.[25,26,43] Compared with a free microtubule ($\mu = 0$ and $\lambda = 0$), the interfacial tension increases the mode velocity [Figs. 2(a)–2(d)]. With the increase in k, the velocities of the second mode for both cases approach to a certain value 835.1 m/s [Figs. 2(a)–2(d)].

The dispersion curve is also compared to that of longitudinal and shearing waves in an infinite medium and the bending wave in a beam [Fig. S1(b)]. The dispersion curve of the first mode is similar to that of the shearing wave in infinite medium, which indicates that the first mode contains mainly the torsional wave mode. Besides, the dispersion curves of the second and third mode are similar to those of longitudinal and bending waves. This suggests that the second and third modes are combinations of the radial wave and the longitudinal wave. For the second mode, when $k < 1$, the longitudinal mode makes up the majority; when $1 < k < 35$, the radial
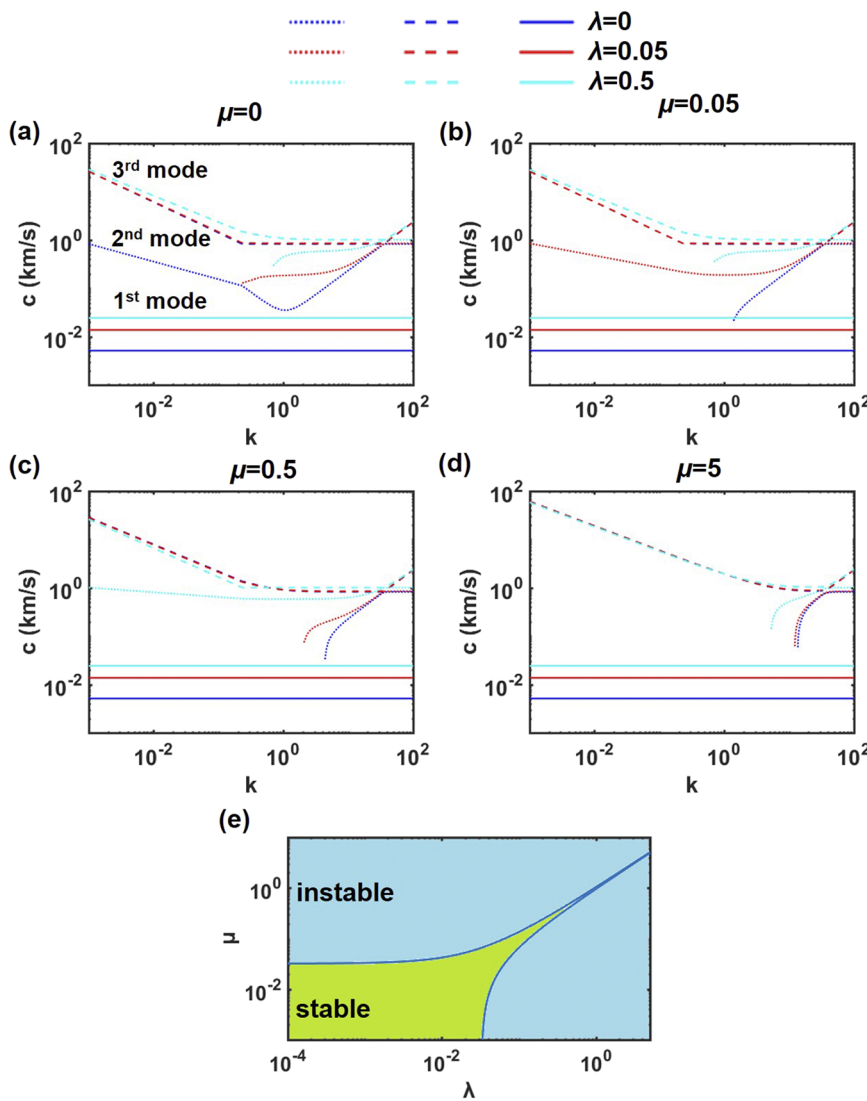

FIG. 2. Influence of interfacial tension and hydrostatic pressure on the dispersion relation for the axisymmetric wave. Increasing the interfacial tension increases wave velocities of all the modes under different hydrostatic pressures. (a) $\mu = 0$: when $\lambda = 0.05$ and 0.5, the second mode becomes unstable. (b) $\mu = 0.05$: when $\lambda = 0$ and 0.5, the second mode becomes unstable. (c) $\mu = 0.5$: when $\lambda = 0$ and 0.05, the second mode becomes unstable. (d) $\mu = 5$: the second mode becomes unstable when $\lambda = 0$, 0.05, and 0.5. (e) Stability phase diagram of second mode: when $|\lambda\text{-}\mu|$ is large enough, the second mode will become unstable in a certain range of k.

mode makes up the majority. When $k > 35$, the longitudinal mode makes up the majority and the velocity remains constant. For the third mode, there is a platform stage when $0.2 < k < 35$ in which the longitudinal mode takes up the majority. In this stage, there is no dispersion. When $k > 35$, the velocity of the third mode increases, consistent with the bending wave in a beam. In this stage, the radial wave takes the majority.

In multi-mode cases, the "quasi-osculation point" is a common phenomenon.[44,45] In the present case, a "quasi-osculation point" exists between the second and third modes when k is about 35 [Figs. 2(a)–2(d)]. Near this point, the dispersion curves of the two modes are close to each other and show a rapid change in gradient. This is because different wave fields (i.e., radial wave, longitudinal wave, and torsional wave) are coupled together, and neighboring modes change their properties (e.g., from the radial wave to longitudinal wave in the second mode) with each other.

To further study how interfacial tension and hydrostatic pressure influence the dispersion curve quantitatively, we compare the dispersion curve when the dimensionless interfacial tension satisfies $\lambda = 0$, $\lambda = 0.05$, and $\lambda = 0.5$ under the situation that the dimensionless hydrostatic pressure takes the value of $\mu = 0$, $\mu = 0.05$, $\mu = 0.5$, and $\mu = 5$, respectively. For reference, the dimensionless interfacial tension between water and hydrophobic matter is $\lambda = 0.0393$ and that between water and hydrophilic matter is $\lambda = 0.0015$,[46] while the dimensionless hydrostatic pressure is $\mu = 0.0037$.[27] Therefore, the range of interfacial tension and hydrostatic pressure examined in this study covers the actual values.

Generally speaking, the increase in interfacial tension will increase the velocities of all modes under different hydrostatic pressures [Figs. 2(a)–2(d)]. Interestingly, in certain situations, the second mode becomes unstable when k lies in the range between 1×10^{-3} and 1.0, and the instability point is related not only to interfacial tension but also to hydrostatic pressure (Fig. 2). According to Eqs. (6) and (8), since the two dimensionless parameters are always coupled together as (λ-μ) except for a few special places, the mode instability is closely related to the combined parameter $|\lambda$-$\mu|$. This parameter represents the difference between dimensionless interfacial tension and dimensionless hydrostatic pressure. When $|\lambda$-$\mu|$ is sufficiently small, there will be no mode instability [Figs. 2(a)–2(c)]. However, when $|\lambda$-$\mu|$ is large enough (bigger than 0.032), the second mode will become unstable in certain ranges of k [Fig. 2(d)]. The phase diagram of Fig. 2(e) displays the critical line between the stable and unstable state of the second mode.

The observed mode instability may be explained as follows. Within a certain range of the dimensionless frequency (which is a real number), the dispersion equation only has complex wave number solution for the second mode. In other words, in this situation, the second mode cannot exist in stable form. Physically, this occurs because the second mode mainly contains the radial wave mode, which is suppressed by the hydrostatic pressure and interfacial tension. When the imaginary part of the wave number of the second mode is positive, the second mode will attenuate along the propagation path. In contrast, when the imaginary part becomes negative, the second mode will diverge along the propagation path.[47] In the current study, for the complex solution, the imaginary part is positive, which denotes that the second mode attenuates along the propagating path. In this study, we focus on the dispersion relation, which is only related to the real solution. The real solution represents

the propagation (not attenuating) mode of the wave structure, while the imaginary part of the complex solution represents the energy attenuation.[47] Therefore, the dispersion curve does not show the attenuation or divergence mode.

B. Non-axisymmetric wave

Equation (12) gives dispersion equations for all three modes of a non-axisymmetric wave. Again, we only consider real wave number solution with stable modes and systematically vary the values of interfacial tension and hydrostatic pressure to quantify how these two parameters influence the dispersion curve. For validation, we compare the theoretical predictions with existing results in the limit when there is no interfacial tension and hydrostatic pressure:[25,26,43] excellent agreement is achieved.

Unlike the axisymmetric situation, the three modes of a non-axisymmetric wave are coupled. To clarify the property of each mode, we compare the dispersion curves of the three modes to those of longitudinal and shearing waves in infinite medium and the bending wave in a beam [Fig. S2(e)]. For the first mode, when $k < 0.1$, the dispersion curve is similar to that of the bending wave, implying that the first mode contains mainly the radial wave mode; when $k > 0.1$, the dispersion curve is similar to that of the shearing wave, indicating that the first mode contains mainly the torsional wave mode. Besides, the dispersion curves of the second and third modes are similar to those of longitudinal and bending waves. This suggests that the second and third modes are combinations of the radial wave and the longitudinal wave. For the second mode, when $k < 1$, the longitudinal mode makes up the majority; when $1 < k < 35$, the radial mode makes up the majority. When $k > 35$, the longitudinal mode makes up the majority and the velocity remains constant. For the second mode, there is a platform stage when $0.2 < k < 35$ in which the longitudinal mode takes up the majority. In this stage, there is no dispersion. When $k > 35$, the velocity of the third mode increases, consistent with the bending wave in a beam. In this stage, the radial wave takes the majority.

For an axisymmetric wave, only one "quasi-osculation point" exists. For a non-axisymmetric wave, however, there exist two "quasi-osculation points," separately between the first and second modes and between the second and third modes. That is because the three modes of the non-axisymmetric wave are coupled together and can be transformed into each other.

To explore the role of interfacial tension, we study the influence of dimensionless interfacial tension λ on the dispersion curve for different modes when $\mu = 0.005$ [Figs. 3(a)–3(c)]. For the first mode with the lowest velocity, when $\lambda = 0$ and $\lambda = 0.05$, the first mode becomes unstable when the dimensionless wave number k is small ($k \approx 1$). Besides, the increase in interfacial tension will increase the steady velocity when k reaches 100. For the second mode with medium velocity, mode instability occurs only when $\lambda = 0$. For the second and third modes, the wave velocity increases as the circumferential wave number n (not near $k = 1$) is increased. However, the increase in λ causes non-monotonic change in wave velocity because the increase in λ causes non-monotonic change in $|\lambda$-$\mu|$ and a positive relation exists between $|\lambda$-$\mu|$ and the velocity of the two modes [Eq. (12)].

To explore the role of hydrostatic pressure, we study the influence of dimensionless hydrostatic pressure μ on the dispersion curve
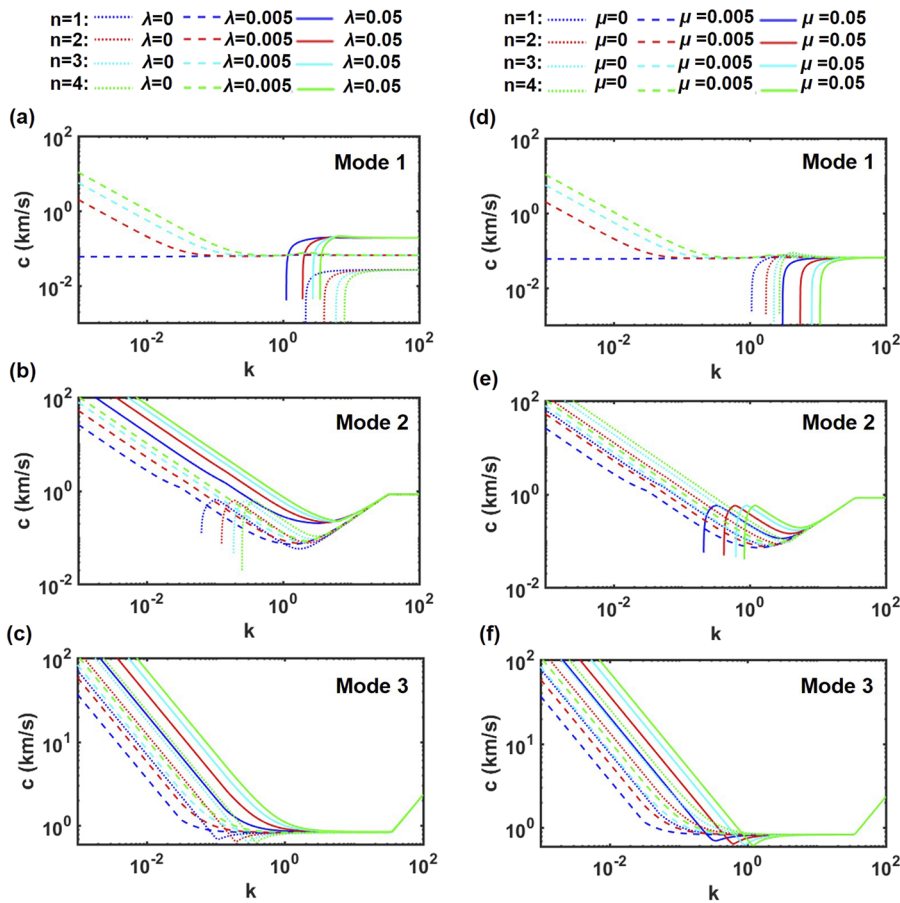
FIG. 3. Influence of interfacial tension and hydrostatic pressure on dispersion relation of a non-axisymmetric wave with angular parameter n = 1, 2, 3, and 4. [(a)–(c)] Influence of dimensionless interfacial tension λ on dispersion relation of modes 1, 2, and 3 when dimensionless hydrostatic pressure μ = 0.005. The increase in λ increases the wave velocity of the first mode but causes non-monotonic change in wave velocity of the second and third modes. [(d)–(f)] Influence of hydrostatic pressure on dispersion relation of modes 1, 2, and 3 when λ = 0.005. Increasing the dimensionless hydrostatic pressure causes slightly decreased wave velocity of the first mode but causes non-monotonic change in wave velocity of the second and third modes. Mode instability happens in both the first and second modes.

for different modes when λ = 0.005 [Figs. 3(d)–3(f)]. For the first mode with the lowest velocity, when μ = 0 and μ = 0.05, the first mode becomes unstable when k is small ($k \approx 1$). For the second mode with a medium velocity, mode instability occurs only when μ = 0.05. With the increase in circumferential wave number n, the wave velocities of all three modes increase. The increase in μ causes increased wave velocity of the first mode and nonmonotonic change in the second and third modes.

The dispersion curves in Figs. 3(a)–3(f) are similar, which means that the effects of interfacial tension and hydrostatic pressure on dispersion are similar. This can be interpreted as follows:

while hydrostatic pressure only generates radial force as shown in Eq. (3), interfacial tension induces both radial force and axial tension. Nonetheless, although interfacial tension has influence on two directions, its influence on the axial direction is not obvious. Therefore, interfacial tension and hydrostatic pressure exhibit similar effects on dispersion.

To explore how interfacial tension and hydrostatic pressure influence the mode instability, we present the phase diagram of the second and third modes [Figs. 4(a) and 4(b)]. Upon varying λ and μ, mode instability occurs in both the second and third modes (Fig. 3) because they both contain the radial wave mode, which is repressed
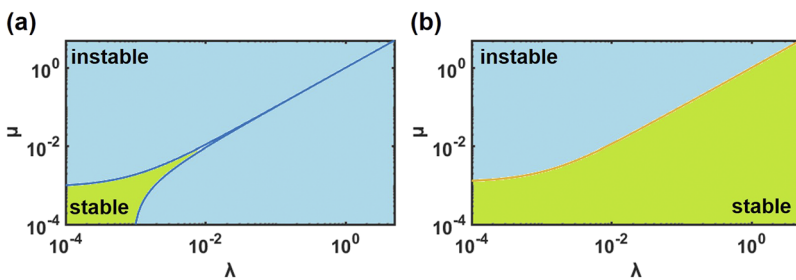

FIG. 4. Phase diagram of stability: (a) first mode and (b) second mode.

by the hydrostatic pressure. For the first mode, mode instability is only related to the value of $|\lambda\text{-}\mu|$. When $|\lambda\text{-}\mu|$ is small enough ($|\lambda\text{-}\mu|$ < 0.001), there is no mode instability in the first mode. As a result, the stable area is restricted in a banding regime, which separates the three parts of the phase diagram [Fig. 4(a)]. However, for the second mode, the phase diagram of mode stability is divided into two parts [Fig. 4(b)]. Only when ($\mu\text{-}\lambda$) is positive and large enough ($\mu\text{-}\lambda$ > 0.001), the second mode becomes unstable.

IV. DISCUSSION

Wave propagation along a microtubule plays critical roles in cell division, cell motility, and signal transmission.[3–5] As the surrounding environment of the microtubule changes, it is likely that the interfacial tension and hydrostatic pressure will also change. Specifically, the change of osmotic environment may change the hydrostatic pressure, and the change of cellular components may change the interfacial tension. Our theoretical model can provide quantitative predictions regarding how interfacial tension and hydrostatic pressure can influence cell division, cell motility, and signal transmission. The change of environment can cause changes of interfacial tension and hydrostatic pressure in cells, which, in turn, will possibly cause the attenuation (a kind of instability) of different modes in microtubules. This may serve as a signal for the cell to modulate its division period and moving path. In signal transmission, for neuron cells, the propagation of action potential is always accompanied by mechanical waves along microtubules in axon.[6,7] According to the theory proposed in the present study, varying the interfacial tension and/or hydrostatic pressure can cause certain modes to attenuate, which, in turn, can disable the propagation of signal with a certain wave number.

Nondestructive testing is a wide group of analysis methods in science and technology to evaluate the properties of a material or component without causing damage.[48] This technique has also been used in cell investigation.[12–14] Since the frequency range (Figs. 2 and 3) (7.8×10^{6}–7.8×10^{12}) covers the frequency of ultrasound imaging in cells (30–50 MHz),[49,50] our study provides guidelines for ultrasound imaging and other non-destructive detections in cells. In cell ultrasound imaging, microtubules can serve as a contrast agent.[12] Mode instability may lead to reduced contrast intensity. By adjusting the osmotic environment or changing the concentration of certain components by drug delivery, hydrostatic pressure and interfacial tension can be controlled so that mode instability can be avoided, thus enhancing the quality of image. Wave propagation in microtubules is also used in other non-destructive detections in cells to obtain information concerning the mechanical properties of cells. Besides detecting the mechanical properties of microtubules, the minimum wave number of certain stable modes can also be used to evaluate hydrostatic pressure and interfacial tension and characterize the relevant properties of the surrounding matter.

Wave propagation in many other microtubule-like capillary structures, e.g., Arabidopsis leaf trichomes,[51,52] auditory hair cells[53,54] and capillary vessel[55] in nature, and carbon nanotubes[56,57] in engineering fields, can also be significant for both biological signal transmission and engineering applications. Although our theoretical model is used to describe the behavior of microtubules, it can be generalized to these microtubule-like capillary structures.

For instance, hair cells are the sensory receptors of both the auditory system and the vestibular system in the ears of all vertebrates. They are sensitive to the sound wave, which can cause mechanotransduction for them to detect the movement in their environment.[58] By adjusting the environment, we may prevent the mode attenuation due to senescence or injuries. In engineering, for nano-electromechanical systems (NEMS), nano-components such as high frequency resonators and oscillators[59,60] are inevitably subjected to the shock wave,[61] which can have an impact on the function of these advices. By adjusting the environment, we can control the interfacial tension and hydrostatic to avoid certain modes. In ultrasound imaging, Intravascular Ultrasound (IVUS)[62] and Intravascular Optical Coherence Tomography (OCT)[63] are common methods to visualize the endothelium of blood vessels in living individuals in which wave propagation in capillary vessels is important for imaging. By adjusting the physiological environment, we can avoid disadvantageous mode attenuation in order to improve the image quality. Active feedback control has enjoyed wide applications in elastic wave metamaterials to control the properties of sound radiation.[64] Inspired by this, we can also utilize active feedback control to tune the stability of wave mode in microtubule-like structures to enhance the quality of the ultrasound image.

Small scale is an important feature at the size of a microtubule. The small scale effect includes the interface effect and discrete effect. In the current work, we mainly consider the interface effect related to small scale instead of the discrete properties related to small scale. As for the discrete properties, there exist a few modified continuum mechanics models (e.g., nonlocal, modified coupled stress, and strain gradient theories) that describe the mechanical behavior related to the small scale characteristic of the discrete effect.[65–70] In wave propagation, although the classical continuum mechanics model presents inaccurate dispersion relation when the wave number is large (>2×10^{8} m^{-1}), accurate dispersion relation can be obtained when the wave number is small (<2×10^{8} m^{-1}).[43] Therefore, although we do not consider the discrete properties related to the small scale in our model, it is suitable for the quantitate study of low frequency (small wave number) waves and the qualitative study of high frequency (large wave number) waves.

V. CONCLUSION

In this study, with the consideration of interfacial tension and hydrostatic pressure, the governing equation of a microtubule is developed based on Flügge's shell theory. The dispersion properties of both axisymmetric wave and non-axisymmetric wave in microtubules are then characterized for the selected values of interfacial tension and hydrostatic pressure. For axisymmetric waves, the velocities of both the first and second modes increase sensitively with the increase in interfacial tension or decrease in hydrostatic pressure, but the third mode is less sensitive. Mode instability is closely related to the difference between dimensionless interfacial tension and hydrostatic pressure. When the difference is sufficiently large, mode instability occurs. For non-axisymmetric waves, the wave velocity is positively correlated with the difference between dimensionless interfacial tension and hydrostatic pressure for the second and third modes, exhibiting a non-monotonic change when increasing either the interfacial tension or the hydrostatic pressure. The change of interfacial tension and hydrostatic pressure causes mode

instability in the first and second modes. In addition, the critical conditions for mode instability are different between the two modes: for the first mode, the stability area (i.e., no mode attenuation) is band-like and for the second mode, the stability area is a semi-infinite area. Since the change of wave velocity and mode instability can reflect the information on the surrounding properties, our results can help understand the role of wave propagation in cell division, mobility, and signal transmission under different environments and provide guidelines for nondestructive testing in cells.

SUPPLEMENTARY MATERIAL

See the supplementary material for detailed derivation of the governing equation of a liquid-filled microtubule. Furthermore, the dispersion relation of an empty microtubule is compared to that of a liquid-filled microtubule. The dispersion relation of a liquid-filled microtubule is also compared to that of longitudinal and shearing waves in infinite medium and the bending wave in a beam.

ACKNOWLEDGMENTS

REFERENCES

[1] H. Li, D. J. Derosier, W. V. Nicholson, E. Nogales, and K. H. Downing, "Microtubule structure at 8 Å resolution," Structure **10**(10), 1317–1328 (2002).

[2] E. Mandelkow and E. M. Mandelkow, "Microtubule structure," Curr. Opin. Struct. Biol. **4**(2), 171–179 (1994).

[3] L. R. Vega and F. Solomon, "Microtubule function in morphological differentiation: Growth zones and growth cones," Cell **89**(6), 825–828 (1997).

[4] T. H. Macrae, "Towards an understanding of microtubule function and cell organization: An overview," Biochem. Cell Biol. **70**(10-11), 835–841 (1992).

[5] J. Avila, "Microtubule functions," Life Sci. **50**(5), 327–334 (1992).

[6] K. Iwasa and I. Tasaki, "Mechanical changes in squid giant axons associated with production of action potentials," Biochem. Biophys. Res. Commun. **95**(3), 1328–1331 (1980).

[7] M. M. Rvachev, "On axoplasmic pressure waves and their possible role in nerve impulse propagation," Biophys. Rev. Lett. **05**(02), 73 (2010).

[8] E. Houliston, D. Carré, J. A. Johnston, and C. Sardet, "Axis establishment and microtubule-mediated waves prior to first cleavage in Beroe ovata," Development **117**(1), 75–87 (1993).

[9] R. C. Brown, B. Lemmon, and H. Nguyen, "The microtubule cycle during successive mitotic waves in the syncytial female gametophyte of ginkgo," J. Plant Res. **115**(6), 491–494 (2002).

[10] C. J. Brokaw, "Bending-wave propagation by microtubules and flagella," Math. Biosci. **90**(1-2), 247–263 (1988).

[11] C. J. Brokaw, "Microtubule sliding in reduced-amplitude bending waves of Ciona sperm flagella: Resolution of metachronous and synchronous sliding components of stable bending waves," Cell Motil. Cytoskeleton **26**(2), 144–162 (1993).

[12] R. Bekeredjian, S. Behrens, J. Ruef, E. Dinjus, E. Unger, M. Baum, and H. F. Kuecherer, "Potential of gold-bound microtubules as a new ultrasound contrast agent," Ultrasound Med. Biol. **28**(5), 691–695 (2002).

[13] O. Wagner, J. Zinke, P. Dancker, W. Grill, and J. Bereiter-Hahn, "Viscoelastic properties of f-actin, microtubules, f-actin/α-actinin, and f-actin/hexokinase determined in microliter volumes with a novel nondestructive method," Biophys. J. **76**(5), 2784–2796 (1999).

[14] M. Triki, A. Duhant, C. Poulin, B. Moulin, C. Archier, T. Antonini, F. Teppe, and W. Knap, "Real-time nondestructive imaging with THz waves," in *2016 21st International Conference on Microwave, Radar and Wireless Communications (MIKON)* (IEEE, 2016).

[15] P. J. D. Pablo, I. A. T. Schaap, F. C. Mackintosh, and C. F. Schmidt, "Deformation and collapse of microtubules on the nanometer scale," Phys. Rev. Lett. **91**(9), 098101 (2003).

[16] D. Sept and F. C. MacKintosh, "Microtubule elasticity: Connecting all-atom simulations with continuum mechanics," Phys. Rev. Lett. **104**(1), 018101 (2010).

[17] C. Y. Wang, C. Q. Ru, and A. Mioduchowski, "Vibration of microtubules as orthotropic elastic shells," Physica E **35**(1), 48–56 (2006).

[18] J. Zhang and S. A. Meguid, "Buckling of microtubules: An insight by molecular and continuum mechanics," Appl. Phys. Lett. **105**(17), 173704 (2014).

[19] M. Kurachi, M. Hoshi, and H. Tashiro, "Buckling of a single microtubule by optical trapping forces: Direct measurement of microtubule rigidity," Cytoskeleton **30**(3), 221 (1995).

[20] M. Kikumoto, M. Kurachi, V. Tosa, and H. Tashiro, "Flexural rigidity of individual microtubules measured by a buckling force with optical traps," Biophys. J. **90**(5), 1687–1696 (2006).

[21] D. J. Needleman, M. Ojedalopez, K. Ewert, J. B. Jones, H. P. Miller, L. Wilson, and C. R. Safinya, "Microtubules buckling and bundling under osmotic stress: A synchrotron X-ray diffraction study probing inter-protofilament bond strength," APS March Meeting Abstracts, 2004.

[22] S. Kasas, C. Cibert, A. Kis, L. Los Rios, B. M. Riederer, L. Forró, G. Dietler, and S. Catsicas, "Oscillation modes of microtubules," Biol. Cell **96**(9), 697–700 (2004).

[23] J. A. Tuszyński, T. Luchko, S. Portet, and J. M. Dixon, "Anisotropic elastic properties of microtubules," Eur. Phys. J. E **17**(1), 29–35 (2005).

[24] S. Kasas, A. Kis, B. M. Riederer, L. Forró, G. Dietler, and S. Catsicas, "Mechanical properties of microtubules explored using the finite elements method," Chemphyschem **5**(2), 252–257 (2004).

[25] X. S. Qian, J. Q. Zhang, and C. Q. Ru, "Wave propagation in orthotropic microtubules," J. Appl. Phys. **101**(8), 084702 (2007).

[26] M. Taj and J. Zhang, "Analysis of wave propagation in orthotropic microtubules embedded within elastic medium by Pasternak model," J. Mech. Behav. Biomed. Mater. **30**, 300–305 (2014).

[27] T. Kitahara, T. Konomi, M. Murata, N. Berg, and P. Wilde, "Influences of gas diffusion layer design parameters on the performance of polymer electrolyte fuel cells," ECS Trans. **5**, 27–36 (2007).

[28] N. Vargaftik, B. Volkov, and L. Voljak, "International tables of the surface tension of water," J. Phys. Chem. Ref. Data **12**(3), 817–820 (1983).

[29] M. Pilhofer, M. S. Ladinsky, A. W. McDowall, G. Petroni, and G. J. Jensen, "Microtubules in bacteria: Ancient tubulins build a five-protofilament homolog of the eukaryotic cytoskeleton," PLoS Biol. **9**(12), e1001213 (2011).

[30] A. M. Wulff and H. Burkhardt, "Mechanisms affecting ultrasonic wave propagation in fluid-containing sandstones under high hydrostatic pressure," J. Geophys. Res.: Solid Earth **102**(B2), 3043–3050, https://doi.org/10.1029/96jb03184 (1997).

[31] M. E. Gurtin and A. I. Murdoch, "Effect of surface stress on wave propagation in solids," J. Appl. Phys. **47**(10), 4414–4421 (1976).

[32] C. Horvath, C. Arratia, and M. L. Cordero, "Measurement of the dispersion relation of a convectively unstable capillary jet under confinement," Phys. Fluids **27**(11), 114103 (2015).

[33] A. Shmyrov, A. Mizev, A. Shmyrova, and I. Mizeva, "Capillary wave method: An alternative approach to wave excitation and to wave profile reconstruction," Phys. Fluids **31**(1), 012101 (2019).

[34] M. Jibu, S. Hagan, S. R. Hameroff, K. H. Pribram, and K. Yasue, "Quantum optical coherence in cytoskeletal microtubules: Implications for brain function," Biosystems **32**(3), 195–209 (1994).

[35] S. Sahu, S. Ghosh, B. Ghosh, K. Aswani, K. Hirata, D. Fujita, and A. Bandyopadhyay, "Atomic water channel controlling remarkable properties

of a single brain microtubule: Correlating single protein to its supramolecular assembly," Biosens. Bioelectron. **47**, 141–148 (2013).

[36]M. H. Köhler, J. R. Bordin, C. F. de Matos, and M. C. Barbosa, "Water in nanotubes: The surface effect," Chem. Eng. Sci. **203**, 54–67 (2019).

[37]M. Whitby and N. Quirke, "Fluid flow in carbon nanotubes and nanopipes," Nat. Nanotechnol. **2**(2), 87–94 (2007).

[38]J. Howard and A. A. Hyman, "Dynamics and mechanics of the microtubule plus end," Nature **422**(6933), 753–758 (2003).

[39]M. Chakraborty, E. V. Tarasovetc, A. V. Zaytsev, M. Godzi, A. C. Figueiredo, F. I. Ataullakhanov, and E. L. Grishchuk, "Microtubule end conversion mediated by motors and diffusing proteins with no intrinsic microtubule end-binding activity," Nat. Commun. **10**(1), 1673 (2019).

[40]D. I. W. Flügge, *Stresses in Shells* (Springer, 1960).

[41]J. Schwaighofer and H. F. Microys, "Orthotropic cylindrical shells under line load," J. Appl. Mech. **46**, 356–362 (1979).

[42]X. Li and Y. Chen, "Transient dynamic response analysis of orthotropic circular cylindrical shell under external hydrostatic pressure," J. Sound Vib. **257**(5), 967–976 (2002).

[43]J. Wang and Y. Gao, "Nonlocal orthotropic shell model applied on wave propagation in microtubules," Appl. Math. Modell. **40**(11-12), 5731–5744 (2016).

[44]A. Levshin and G. Panza, "Caveats in multi-modal inversion of seismic surface wavefields," Pure Appl. Geophys. **163**(7), 1215–1233 (2006).

[45]D. De Nil, "Characteristics of surface waves in media with significant vertical variations in elasto-dynamic properties," J. Environ. Eng. Geophys. **10**(3), 263–274 (2005).

[46]A. H. Demond and A. S. Lindner, "Estimation of interfacial tension between organic liquids and water," Environ. Sci. Technol. **27**(12), 2318–2331 (1993).

[47]J. L. Rose and P. Nagy, *Ultrasonic Waves in Solid Media* (Cambridge University Press, 2000).

[48]L. Cartz, *Nondestructive Testing* (ASM International, 1995).

[49]G. J. Czarnota, M. C. Kolios, J. Abraham, M. Portnoy, F. P. Ottensmeyer, J. W. Hunt, and M. D. Sherar, "Ultrasound imaging of apoptosis: High-resolution non-invasive monitoring of programmed cell death *in vitro*, *in situ* and *in vivo*," Br. J. Cancer **81**(3), 520–527 (1999).

[50]G. J. Czarnota, M. C. Kolios, J. W. Hunt, and M. D. Sherar, "Ultrasound imaging of apoptosis. DNA-damage effects visualized," Methods Mol. Biol. **203**, 257–277 (2002).

[51]S. Liu, J. Jiao, T. J. Lu, F. Xu, B. G. Pickard, and G. M. Genin, "Arabidopsis leaf trichomes as acoustic antennae," Biophys. J. **113**(9), 2068–2076 (2017).

[52]L. H. Zhou, S. B. Liu, P. F. Wang, T. J. Lu, F. Xu, G. M. Genin, and B. G. Pickard, "The Arabidopsis trichome is an active mechanosensory switch," Plant, Cell Environ. **40**(5), 611–621 (2016).

[53]X. P. Liu, K. R. Koehler, A. M. Mikosz, E. Hashino, and J. R. Holt, "Functional development of mechanosensitive hair cells in stem cell-derived organoids parallels native vestibular hair cells," Nat. Commun. **7**, 11508 (2016).

[54]M. Beurg, A. C. Goldring, A. J. Ricci, and R. Fettiplace, "Development and localization of reverse-polarity mechanotransducer channels in cochlear hair cells," Proc. Natl. Acad. Sci. U. S. A. **113**(24), 6767–6772 (2016).

[55]W. Wiedemair, Z. Tukovic, H. Jasak, D. Poulikakos, and V. Kurtcuoglu, "On ultrasound-induced microbubble oscillation in a capillary blood vessel and its implications for the blood-brain barrier," Phys. Med. Biol. **57**(4), 1019–1045 (2012).

[56]S. Henley, *Carbon Nanotubes (CNTs)* (Springer, The Netherlands, 2012).

[57]P. S. Dorozhkin, S. V. Tovstonog, D. Golberg, J. Zhan, Y. Ishikawa, M. Shiozawa, H. Nakanishi, K. Nakata, and Y. Bando, "A liquid-Ga-filled carbon nanotube: A miniaturized temperature sensor and electrical switch," Small **1**(11), 1088–1093 (2005).

[58]E. A. Lumpkin, K. L. Marshall, and A. M. Nelson, "Cell biology of touch," J. Cell Biol. **191**(2), 237–248 (2010).

[59]P. G. Collins, A. Zettl, H. Bando, A. Thess, and R. E. Smalley, "Nanotube nanodevice," Science **278**(5335), 100–102 (2007).

[60]Q. Zheng and Q. Jiang, "Multiwalled carbon nanotubes as gigahertz oscillators," Phys. Rev. Lett. **88**(4), 045503 (2002).

[61]H. Shen, "Wave propagation in carbon nanotube intramolecular junctions: Finite element calculations," Mol. Phys. **113**(7), 753–763 (2015).

[62]H. M. Garcìagarcìa, B. D. Gogas, P. W. Serruys, and N. Bruining, "IVUS-based imaging modalities for tissue characterization: Similarities and differences," Int. J. Cardiovasc. Imag. **27**(2), 215–224 (2011).

[63]H. G. Bezerra, M. A. Costa, G. Guagliumi, A. M. Rollins, and D. I. Simon, "Intracoronary optical coherence tomography: A comprehensive review: Clinical and research applications," JACC: Cardiovasc. Interventions **2**(11), 1035–1046 (2009).

[64]Z. H. He, Y. Z. Wang, and Y. S. Wang, "Active feedback control on sound radiation of elastic wave metamaterials," AIAA J. **57**(10), 4536–4547 (2019).

[65]B. Akgöz and Ö. Civalek, "Application of strain gradient elasticity theory for buckling analysis of protein microtubules," Curr. Appl. Phys. **11**(5), 1133–1138 (2011).

[66]Y. Z. Wang, H. T. Cui, F. M. Li, and K. Kishimoto, "Effects of viscous fluid on wave propagation in carbon nanotubes," Phys. Lett. A **375**(24), 2448–2451 (2011).

[67]B. Akgöz and Ö. Civalek, "Mechanical analysis of isolated microtubules based on a higher-order shear deformation beam theory," Compos. Struct. **118**, 9–18 (2014).

[68]H. S. Shen, "Nonlinear analysis of lipid tubules by nonlocal beam model," J. Theor. Biol. **276**(1), 50–56 (2011).

[69]H. S. Shen, "Nonlinear vibration of microtubules in living cells," Curr. Appl. Phys. **11**(3), 812–821 (2011).

[70]Y. Z. Wang, F. M. Li, and K. Kishimoto, "Wave propagation characteristics in fluid-conveying double-walled nanotubes with scale effects," Comput. Mater. Sci. **48**(2), 413–418 (2010).

[71]T. Young, "III. An essay on the cohesion of fluids," Philos. Trans. R. Soc. London **95**, 65 (1805).

[72]A. Kis, S. Kasas, B. Babić, A. J. Kulik, W. Benoît, G. A. Briggs, C. Schönenberger, S. Catsicas, and L. Forró, "Nanomechanics of microtubules," Phys. Rev. Lett. **89**(24), 248101 (2002).